Advanced characterization of SiC devices by optical beam induced current (OBIC): Experimental and simulation results

Dominique Planson, Dominique Tournier, Camille Sonneville, Pascal Bevilacqua, Luong Viet Phung, Hervé Morel

Advanced characterization of SiC devices by Optical Beam Induced Current (OBIC): experimental and simulation results

Dominique PLANSON*, Dominique TOURNIER, Camille SONNEVILLE*, Pascal BEVILACQUA*, Luong Viet PHUNG*, Hervé MOREL***

*Univ Lyon, INSA Lyon, Ecole Centrale de Lyon, Université Claude Bernard Lyon 1, CNRS, Ampère, F-69621, Villeurbanne, France

** Caly Technologie, F-69621, Villeurbanne, France

***dominique.planson@insa-lyon.fr**

***camille.sonneville@insa-lyon.fr, *pascal.bevilacqua@insa-lyon.fr, *luong-viet.phung@insa-lyon.fr, *herve.morel@insa-lyon.fr, **dominique.tournier@insa-lyon.fr**

***Abstract*— Wide-bandgap semiconductors, such as silicon carbide (SiC), gallium nitride (GaN), and diamond (C), have proven to outperform traditional silicon (Si) based power electronic devices. However, the peripheral protection of these wide-bandgap devices requires careful design to handle high voltage effectively. This article highlights the potential of using the Optical Beam Induced Current (OBIC) technique to analyze the effectiveness of different protection methods and provide valuable feedback to device designers regarding peripheral termination efficiency. Designers need simulations representative of the measurement, In this article a finite element simulation is used to determine the induced current as a function of the position of the optical beam.**

***Firstly a theoretical approach will be presented to introduce the OBIC method. Subsequently, the electro-optical characterization technique is applied to a PiN diode protected by narrow field rings.**

***The article also showcases new results obtained from components with new-generation peripheral protection, demonstrating the continuous progress in this field.**

Overall, this article highlights the significance of the OBIC technique in evaluating the effectiveness of peripheral protection methods for wide-bandgap semiconductors, particularly SiC devices. By providing valuable insights into the electric field's spatial distribution, this technique aids in optimizing device design and improving overall performance. Finite element simulations in relation to the characteristics of the UV beam and its scanning across the surface of the component help to assess the geometric parameter impact on the electrical results.

Keywords—power device, periphery protection, Silicon Carbide; bipolar diode, field ring, OBIC, simulation.

1. Introduction

Silicon carbide (SiC), gallium nitride (GaN), and diamond (C) are examples of wide bandgap semiconductor materials with exceptional properties for a variety of applications, particularly for high-voltage devices [1][2][3]. Ultrahigh voltage devices (>10 kV) will become more and more important in the near future for modern power grids and High-Voltage Direct Current (HVDC) transmission systems [4][5][6]. Effective peripheral protections are essential to maximizing the advantages of wide-bandgap semiconductor materials and preventing these high-voltage devices from premature breakdown [7][8][9]. To evaluate the effectiveness of peripheral protection, this paper will show how the OBIC technique can be applied by examining the electric field distribution inside the device structure, specifically at the junction periphery. The OBIC approach requires safety measures like a vacuum chamber and the transmission of the optical beam through an optical window [10]. Section 1 briefly describes the principle of OBIC and also the structure of bipolar diodes. The second section employs our improved OBIC setup to characterize lower voltage bipolar diodes with very narrow field ring spacing as a periphery protection. The last part of this paper shows the simulation results obtained from the finite element simulator Sentaurus Synopsys [11]. After a precise description of the experimental bench and the diode structure, the simulator can reproduce the electrical and physical behavior of the UV beam scanning. This makes possible to optimize the geometric parameters of the diode protection to increase its voltage withstand capability right from the design stage. Simulation of the current optically induced by a laser has already been studied on HgCdTe photodiodes [12], but this paper focuses on silicon carbide power diodes.

2. OBIC principle

Silicon diodes protected by field rings have been studied using this method [13] [14]. In order to create electron-hole pairs (EHPs) inside the semiconductor, a focused laser beam is utilized as shown in Figure 1. The surface of the device under test (DUT) is scanned with the laser spot at a chosen pitch (usually 200 nm), while the current is measured thanks to a SMU (Source Measurement Unit). The induced current is then mapped in 2-directions (X and Y) or just for one line in a given direction. The intensity of the photo-generated current is linked to the intensity of the electric field and therefore to the reverse voltage applied to the DUT. The specific OBIC bench has already been described in [15][16][17][18].

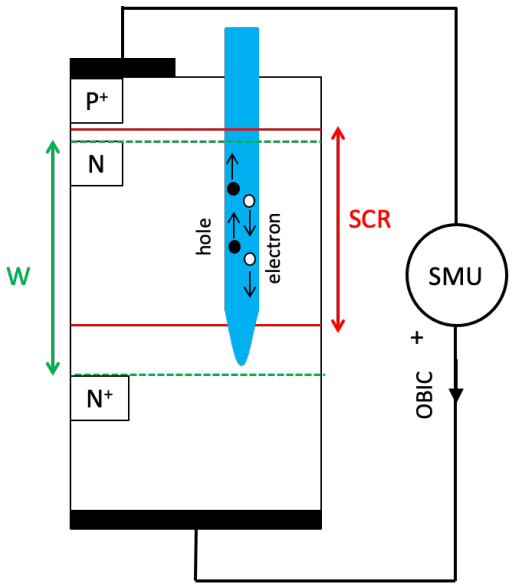

Fig. 1: Plane-parallel infinite PN junction reverse biased by an SMU (Source Measurement Unit). The n-epilayer's thickness is represented by W, and the borders of the space charge region (SCR) are shown in red.

A 349 nm UV pulsed laser is utilized in the micro-OBIC experimental setup to generate electron-hole pairs (EHPs). In order to get a focused laser spot with a diameter of around 1-4 µm, as depicted in Figure 2, a set of appropriately adjusted optics (beam expander, microscope objective, etc.) is fitted on the beam path. The sample is set up on a motorized stage, and LabView is used to manipulate the focal point's position (i.e., automatically on X, Y, Z, and theta manually).

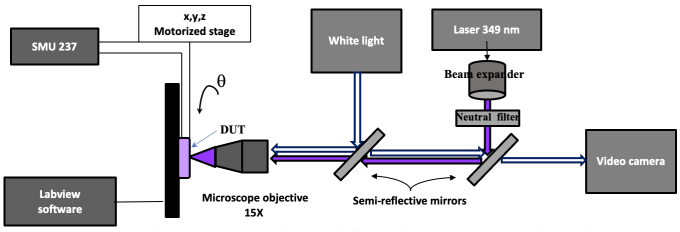

Fig. 2: Schematic representation of the micro-OBIC testbench.

The diode under test placed (under air) can be reverse biased by applying a voltage of up to 500 V using the Keithley 237 SMU.

3. Description of the diode

Figure 3-a illustrates the DUT's cross section as well as its periphery. Thickness of the epilayer is 14.8 µm, doped with n-type (6×10^{15} cm^{-3}). The field rings, which were carefully designed by Caly Technologies, are created simultaneously with the main junction using ion implantation.

As illustrated in Figure 3-b, the metallized anode contact has a square shape, measuring 200 µm by 300 µm on the side and 200 µm on the corner curvature radius.

By scanning the outer edge of the biased diode, this non-destructive method allows to measure OBIC currents and evaluate the effectiveness of peripheral protection. As the electric field within the structure intensity rises, so does the OBIC current. Neither on the metallization nor far from the diode's edge is there any OBIC current.

By giving an insight into the electric field along the peripheral region, OBIC current profiles are valuable data to track down process variation and/or to maximise the breakdown voltage. As seen in Figure 3-a, the diode is shielded by 22 field rings, which are spaced apart increasingly (0.07 µm from one ring to the next). The first ring and the main junction are separated by 1.2 µm. Every ring has the same width, measuring 1.5 µm.

Comparing the distances extracted from OBIC signal and CAD design gives a relatively small difference/gap lower than 3% illustrating the good accuracy of the setup and methodology, given the spot size of 200 nm and the mechanical displacement resolution.

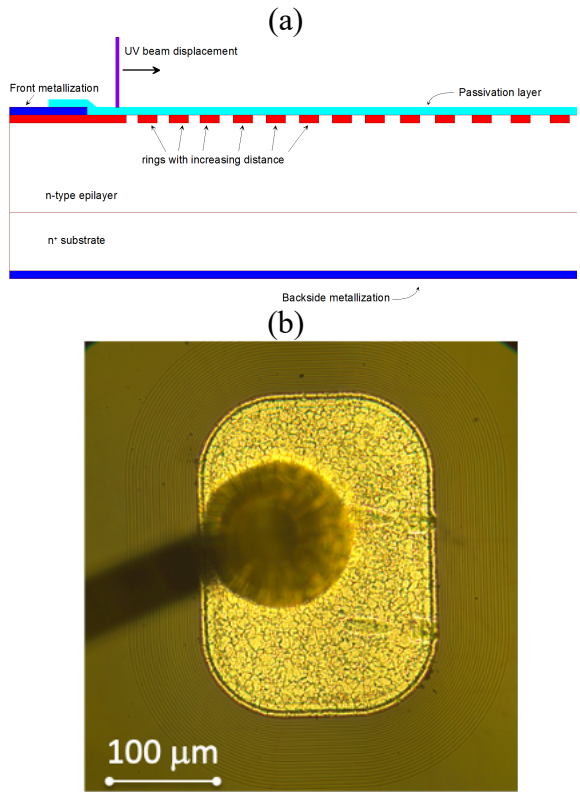

Fig. 3. a) Schematic showing the half-vertical PiN diodes shielded by 22 field rings. b) picture of the diode with the gold ball bonding of 50 µm in diameter.

As illustrated in Figure 4, reverse blocking leakage current on-wafer measurements of the device revealed a stable blocking voltage up to 1.7 kV inside a vacuum probing chamber.

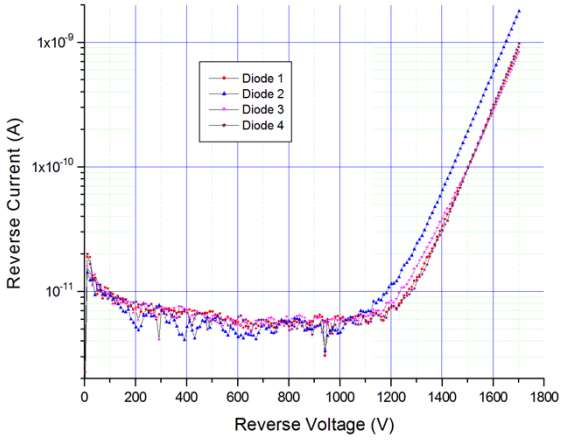

Fig. 4. Characteristic of the reverse leakage current in the vacuum chamber. The measurements have been performed on 4 different samples of the same diode up to 1700 V.

4. OBIC measurements

Several OBIC currents can be compared to one another by rescanning the same location at different reverse voltages (up to 500 V) applied to the same diode, as illustrated in Figure 5. Because of the increased electric field caused by an increase in reverse voltage, the OBIC current also increases at the same location. Additionally, the expansion of the space charge region with increasing reverse voltage and the function of outer field rings, which attest to the carefully designed peripheral protection design, are visible.

The number of OBIC peaks increases in accordance with the reverse voltage. From 20 µm to 97 µm, every maximum is associated with the existence of a ring, as mentioned in [19]; more specifically, it is situated at the periphery of every ring intersection. µ-OBIC makes the presence of the rings more evident as the reverse voltage rises. In fact, the higher the electric field, the greater the generation of carriers and the greater the number of rings visible by OBIC. Very close rings (between 1.2 µm for the first ring and 2.67 µm for the last ring) are present in these measurements up to 500 V. For a 500 V reverse voltage, one can count all 22 field rings in addition to an additional peak for the main junction's border.

The maximum amplitude doesn't significantly increase as voltage changes. The spacing between the peaks is entirely consistent with the ring arrangement as depicted in Table 1 and Figure 5. According to its left lateral edge, which faces the main junction when viewed from the cross-section shown in Figure 3-a, Table 1 indicates the position of each ring. For every left lateral edge, the amplitude of the OBIC signal is provided. When comparing Table 1 data with the OBIC profile extracted from the experimental bench displayed in Figure 5, every profile dip precisely aligns with each ring left lateral edge. Diode was the source of all the data in the current table, which was extracted under a bias of 500 V.

Table 1. Ring mask layout distance from the main junction and the corresponding OBIC signal values.

Ring number	**1**	**2**	**3**	**4**	**5**	**6**	**7**	**8**	**9**	**10**	**11**
CAD	1.2	3.97	6.81	9.72	12.7	15.75	18.87	22,06	25,32	28,65	32,05
Measure	1,19	3,99	6,99	9,79	12,79	16	18,8	22,21	25,38	28,79	32,2
Gap %	0,8%	-0,5%	-2,6%	-0,7%	-0,7%	-1,6%	0,4%	-0,7%	-0,2%	-0,5%	-0,5%

Comparing the distances extracted from OBIC signal and CAD design gives a relatively small difference/gap lower than 3% illustrating the good accuracy of the setup and methodology, given the spot size of 200nm and the mechanical displacement resolution.

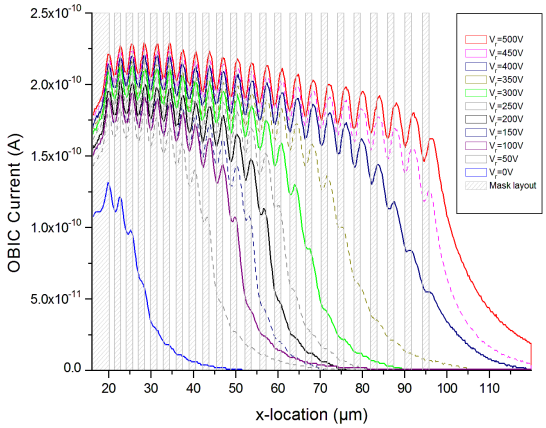

Fig. 5. OBIC currents for various reverse voltages (ranging from 0 V to 500 V by 50 V step) at the diode periphery. The grey color corresponds to the mask layout with the ring spacing.

4. Simulation results

Two-dimensional simulations are performed using Sentaurus Device [11] on the structure shown in Figure 3.a thanks to a properly developed SiC model. True doping levels and dimensions are considered in the device structure description as shown in Figure 6 featuring 22 guard rings. The distance between the rings and the width of the rings are both in agreement with the geometry of the produced components. The time-domain simulation starts by an initialization step followed by a transient voltage ramp which gradually reverse-biased the device. The ramp stops at a final voltage respectively set at 100, 200, 300 and 400 V. For each of these, a carefully built UV beam (Fig. 7) is scanned from the anode electrode to the right outer edge of the structure. During this scanning step, optics models are enabled, and the quantum efficiency is set at 1. Resolution mode is switched to quasi-stationary when optical simulations are computed. The parameters of the UV optical beam (length, width, penetration depth, optical power density) are defined in accordance with the experimental results and also from [20] (Fig. 7). The Gaussian shape is then correctly reproduced thanks to the fine local mesh. The spot displacement is moved in 200 nm, just like the experimental displacement. Figures 8 shows one of the two extreme positions of the laser spot (from the anode outwards).

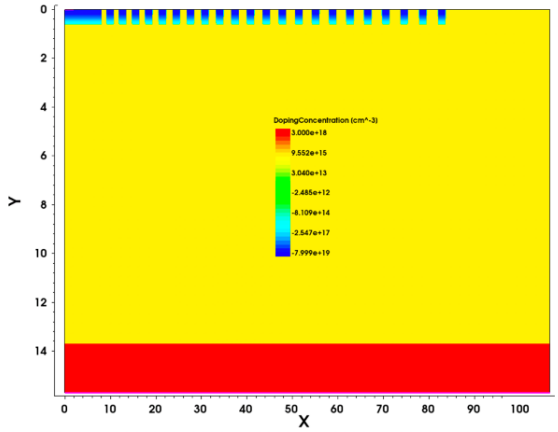

Fig. 6. Cross-sectional view of the half-structure of the diode with its 22 guard rings.

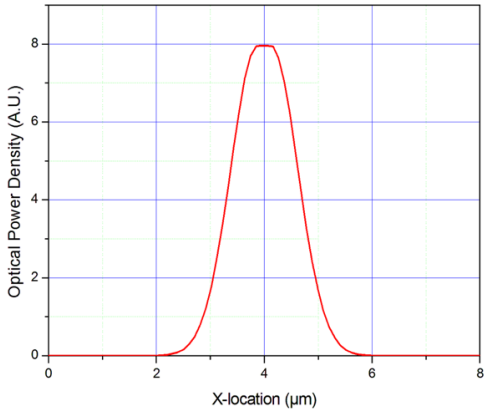

Fig. 7. Optical power density lateral profile extracted from simulation at device surface. The x-axis is given in micrometer. The present profile is centered at 4 µm

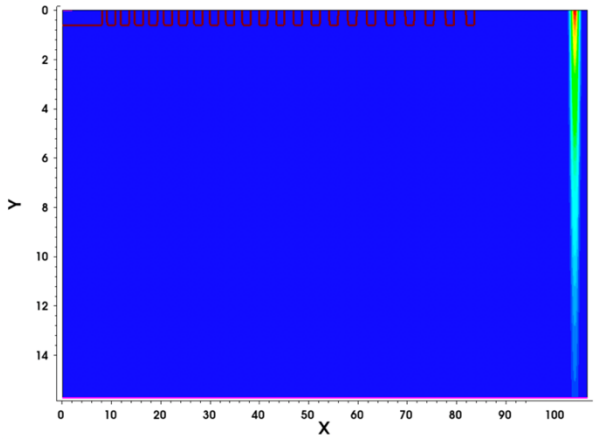

Fig. 8. Representation of the optical power density in the diode x=104) of the Gaussian beam. The shot has been taken at the end of a lateral scanning. The junction lines are shown in brown for both the main junction and the 22 rings.

Figure 9 plots the potential distribution in the structure along the x-axis. As one moves away from the anode, the electric potential describes a staircase pattern where a leap in its value is followed by a plateau. The former is the usual behavior in a n region while the latter is attributed to a guard ring that sets a fixed potential along its width. As the reverse voltage is increased, more and more rings are revealed as the OBIC signal mirrors the electric field thanks to the generation rate of EHPs. At a voltage of 400 V, 9 rings are revealed.

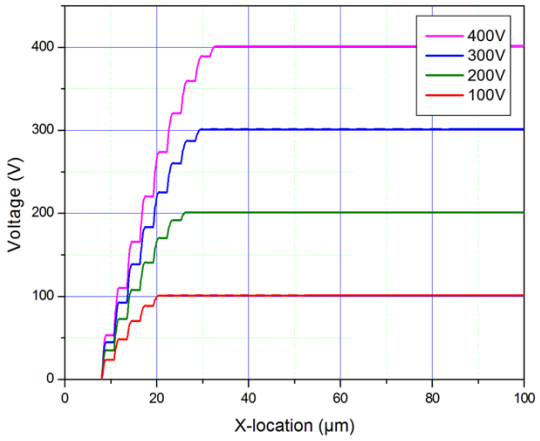

Fig. 9. Equipotential distribution along the structure. The voltage step is 100 V.

For each of the reverse voltages applied to the diode, the simulator computes the current optically induced by scanning the surface from the center outwards. The OBIC currents as a function of position for the different voltages are plotted in Figures 10a and b.

Figures 10-a and 10-b show the simulated OBIC current for one scan of the spot for different reverse voltages applied to the diode. The amplitude of the signal increases with the voltage and so does the lateral extension. This is consistent with experimental measurements. The rings are revealed as the reverse voltage increases. There are 9 variations for 8 rings for the reverse voltage of 400 V, as there is also the edge of the P^+ junction to consider. The signal decay corresponds to the diffusion length outside the space charge zone.

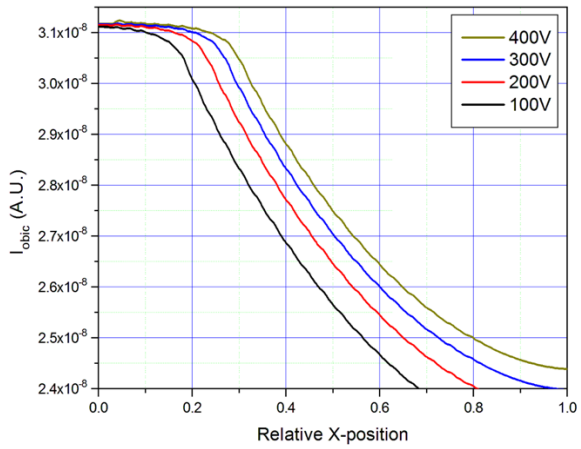

(a)

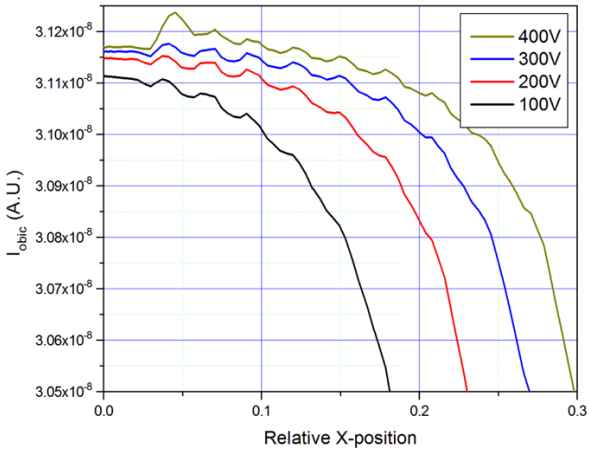

(b)

Fig. 10. Distribution of OBIC current versus reduced x-position for different voltage (from 100V up to 400V). (a): full scale, (b): zoom-in close to the anode electrode. The abscissa scale corresponds to one hundredth of the actual distance (using a reduced variable).

The general observation is that the simulated current looks like the measured current.

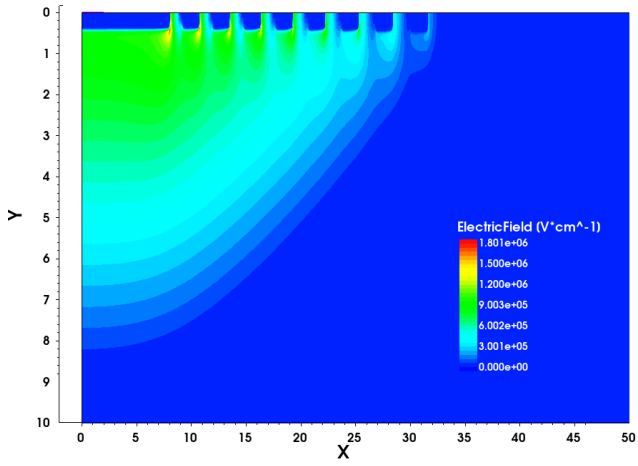

Fig. 11. Electric field distribution in the diode at 400 V reverse bias.

Figure 11 shows the distribution of the electric field along the guard rings for a reverse voltage of 400 V. The maximum value of the electric field is 1.8 MV/cm, which is still far from its critical value. This is due to the reverse voltage which is well below to the maximum value supported by the diode (1700 V). The maximum electric field is to the right of each ring like the experimental OBIC signal which also peaks to the right of each ring. It is easy to see that the electric field is almost zero in the rings, as they are equipotential.

However, differences can still be spotted between experiments and simulations. While experimental data suggest the presence of the 22 rings at 400 V, simulations show otherwise since only 8 rings properly appear on simulations results. Further improvements may be done like more accurate carrier lifetimes, better reproduction of UV beam penetration depth as well as adjusting the depth of 1D data extraction.

5. Conclusion

The OBIC measurements on field rings protected bipolar diodes at various voltages are presented in this paper. Even with the small spacing between each ring, JTE rings are clearly visible in these experiments, indicating that this OBIC test-bench has a good spatial resolution. The study would then be interestingly concluded by measurements at higher reverse bias under vacuum, thereby being closed to the device breakdown voltage of 1 700 V.

The simulation results are fully comparable with the experimental results, enabling us to trace the electric field inside the structure and help the designer to properly optimize his periphery protection.

The approach used in this paper, based on µ-OBIC measurements supplemented by finite element simulations, could also be used for other wide bandwidth semiconductor materials such as GaN, Ga_2O_3, diamond, etc.

Acknowledgments.

The authors would like to thank Pierre Brosselard for measurements in the vacuum chamber of the diodes. The authors would like also to thank Juline Valette for her invaluable help in setting up the finite element simulations.

References

[1] K. Shenai, R. Scott, B.J. Baliga, “Optimum Semiconductors for high-power electronics” IEEE Transactions on Electron Devices, Vol. 36, n°9, pp. 1811-1823, 1989. Doi: 10.1109/16.34247

[2] C. Raynaud, D. Tournier, H. Morel, D. Planson, “Comparison of high voltage and high temperature performances of wide bandgap semiconductors for vertical power devices” Diamond & Related Materials vol.19 p. 1-6, 2010. DOI: 10.1016/j.diamond.2009.09.015

[3] T. Mizushima, K. Takenaka, H. Fujisawa, T. Kato, S. Harada, Y. Tanaka, M. Okamoto, M. Sometani, D. Okamoto, N. Kumagai, S. Matsunanaga, T. Deguchi, M. Arai, T. Hatakeyama, Y. Makifuchi, T. Araoka, N. Oose, T. Tsutsumi, M. Yoshikawa, K. Tatera, A. Tanaka, S. Ogata, K. Nakayama, T. Hayashi, K. Asano, M. Harashima, Y. Sano, E. Morisaki, M. Takei, M. Miyajima, H. Kimura, A. Otsuki, Y. Yonezawa, K. Fukuda, H. Okumura and T. Kimoto, “Dynamic Characteristics of large current capacity module using 16-kV Ultrahigh voltage SiC Flip-type n-channel IE-IGBT” Proc. Int. Symp. On Power Semiconductor Devices & IC’s, pp 277-280, 2014. DOI: 10. 10.1109/ISPSD.2014.6856030

[4] J. Millán, P. Godignon, X. Perpiñà, A. Pérez-Tomás, J. Rebollo, “A Survey of Wide Bandgap Power Semiconductor Devices” IEEE Transactions on Power Electronics Year: Volume: 29, Issue: 5 Pages: 2155 – 2163, 2014. DOI: 10.1109/TPEL.2013.2268900

[5] K. Fukuda, D. Okamoto, M. Okamoto, T. Deguchi, T. Mizushima, K. Takenaka, H. Fujisawa, S. Harada, Y. Tanaka, Y. Yonezawa, T. Kato, S. Katakami, M. Arai, M. Takei, S. Matsunaga, K. Takao, T. Shinohe, T. Izumi, T. Hayashi, S. Ogata, K. Asano, H. Okumura, T.

Kimoto, “Development of Ultrahigh-Voltage SiC Devices” IEEE Transactions on Electron Devices, Volume: 62, Issue: 2, Pages: 396 – 404, 2015. DOI: 10.1109/TED.2014.2357812.

[6] N. Kaji, H. Niwa, J. Suda, T. Kimoto, “Ultrahigh-Voltage SiC p-i-n Diodes With Improved Forward Characteristics”, IEEE Transactions on Electron Devices, Volume: 62, Issue: 2, Pages: 374 – 381, 2015. DOI: 10.1109/TED.2014.2352279.

[7] R. Perret, “Power Electronics Semiconductor Devices”, Ed. Wiley-ISTE, ISBN: 978-1-848-21064-6, 2009.

[8] W. J. Choyke, H. Matsunami, G. Pensl, “Silicon Carbide: Recent Major Advances”, Ed. Springer Science & Business Media, ISBN: 978-3-642-18870-1, 2003.

[9] P. Godignon, J. Montserrat, J. Rebollo, D. Planson “Edge Terminations for 4H-SiC Power Devices: A Critical Issue” Materials Science Forum Vol. 1062, pp 570-575, 2022. doi:10.4028/p-lom714.

[10] D. Planson, B. Asllani, H. Hamad, M.-L. Locatelli, L. Wei, C. Raynaud, P. Bevilacqua, L.V. Phung, Near breakdown voltage optical beam induced current (OBIC) on 4H-SiC bipolar diode, Materials Science Forum Vol. 924 (2018) pp 577-580. https://doi.org/10.4028/www.scientific.net/msf.924.577.

[11] Sentaurus Device User Guide Version V-2023.09, http://www.synopsys.com/home.aspx

[12] Yin, F., Hu, W.D., Zhang, B. et al. Simulation of laser beam induced current for HgCdTe photodiodes with leakage current. Opt Quant Electron 41, 805–810 (2009). https://doi.org/10.1007/s11082-010-9394-y.

[13] R. Stengl, “High-voltage planar junctions investigated by the OBIC method”, IEEE Transactions on electron devices, vol. ED-34, no. 4, pages 911-919, 1987. DOI: 10.1109/T-ED.1987.23015.

[14] T. Flohr and R. Helbig, “Determination of minority-carrier lifetime and surface recombination velocity by Optical-Beam-Induced-Current measurements at different light wavelengths,” J. Appl. Phys., Vol. 66, Issue 7, pp. 3060-3065, 1989. https://doi.org/10.1063/1.344161.

[15] C. Raynaud, D.-M. Nguyen, N. Dheilly, D. Tournier, P. Brosselard, M. Lazar, D. Planson “Optical beam induced current measurements: principles and applications to SiC device characterization”, Phys. Status Solidi A 206, n°10, 2273-2283, 2009. https://doi.org/10.1002/pssa.200825183.

[16] H. Hamad, C. Raynaud, P. Bevilacqua, S. Scharnholz, D. Planson, Materials Science Forum Vols. 821-823 (2015),p.223-228. https://doi.org/10.4028/www.scientific.net/MSF.821-823.223

[17] C. Sonneville, D. Planson, L.-V. Phung, P. Bevilacqua, B. Asllani “Interest of using a micro-meter spatial resolution to study SiC semi-conductor devices by Optical Beam Induced Current (OBIC)”, Materials Science Forum Vol. 1004, pp 290-298, 2020. https://doi.org/10.4028/www.scientific.net/MSF.1004.290.

[18] D. Planson, C. Sonneville, P. Bevilacqua, L V Phung, B. Asllani, D. Tournier, P. Brosselard “4H-SiC PiN diode protected by narrow fields rings investigated by the OBIC method”, Materials Science Forum Vol. 1062, 2022. https://doi.org/10.4028/p-2ch22f.

[19] P. Godignon, J. Montserrat, J. Rebollo, D. Planson ”Edge Terminations for 4H-SiC Power Devices: A Critical Issue” Materials Science Forum Vol. 1062 (2022) pp 570-575. doi:10.4028/p-lom714.

[20] S.G. Sridhara, T.J. Eperjesi, R.P. Devaty, W.J. Choyke "Penetration depths in the ultraviolet for 4H, 6H an 3C silicon carbide at seven common laser pumping wavelengths", Materials Science and Engineering: B, Vol. 61-62, page 229,233. https://doi.org/10.1016/S0921-5107(98)00508-X.